N-(2-(Dimethylamino)Ethyl)-4-^{18}F-Fluorobenzamide: A Novel Molecular Probe for High-Contrast PET Imaging of Malignant Melanoma

Ayoung Pyo[1], Hyeon Sik Kim[1], Hyung Seok Kim[2], Misun Yun[3], Dong-Yeon Kim[1], and Jung-Joon Min[1]

[1]Department of Nuclear Medicine, Chonnam National University Medical School and Hwasun Hospital, Hwasun, Korea; [2]Department of Forensic Medicine, Chonnam National University Medical School, Hwasun, Korea; and [3]Microbiology and Functionality Research Group, Research and Development Division, World Institute of Kimchi, Gwangju, Korea

Malignant melanoma is an aggressive and serious form of skin cancer, with prognosis and treatment outcome depending heavily on the clinical stage of the disease at the time of diagnosis. Here, we synthesized a novel ^{18}F-labeled benzamide derivative to target melanoma and then evaluated its biologic characteristics in small-animal models. **Methods:** N-(2-(dimethylamino)ethyl)-4-^{18}F-fluorobenzamide (^{18}F-DMFB) was synthesized by reaction of N-succinimidyl 4-^{18}F-fluorobenzoate with N,N-dimethylethylenediamine. The binding affinity of ^{18}F-DMFB was measured in B16F10 (mouse melanoma) cells with or without L-tyrosine. Small-animal PET imaging with ^{18}F-DMFB was performed on B16F10 xenograft and metastasis mouse models. **Results:** The overall non–decay-corrected radiochemical yield of ^{18}F-DMFB was approximately 10%–15%. Uptake of ^{18}F-DMFB was melanin-specific, as cellular uptake in B16F10 increased more than 18-fold in the presence of L-tyrosine. Biodistribution studies revealed that ^{18}F-DMFB accumulated, and was retained, in B16F10 xenografts for 120 min (10, 30, 60, and 120 min: 9.24, 10.80, 13.0, and 10.59 percentage injected dose/g, respectively) after radiotracer injection. Liver uptake of ^{18}F-DMFB decreased from 10 to 120 min and showed fast clearance (10, 30, 60, and 120 min: 11.19, 5.7, 2.47, and 0.4 percentage injected dose/g). Furthermore, ^{18}F-DMFB allowed visualization of metastatic lesions immediately after injection and was retained in lesions for over 60 min, with a high tumor-to-background ratio. **Conclusion:** ^{18}F-DMFB demonstrated a high melanin-targeting ability and tumor-specific tumor uptake in both primary and metastatic lesions in animal models bearing malignant melanoma. ^{18}F-DMFB may be a potential PET imaging agent for melanoma.

Key Words: malignant melanoma; metastasis; ^{18}F-labeled benzamide derivative; PET; molecular imaging

Malignant melanoma is the most aggressive type of skin cancer, with the highest rates of metastasis and mortality (1,2). The incidence of metastatic melanoma has increased over the past 3 decades, with a mortality rate that continues to rise more quickly than that of most other cancers (3). In the last few years we have witnessed an unparalleled change in treatment options for patients with metastatic melanoma, including development of new therapeutic strategies such as targeted therapies and immunotherapies, which have improved patient prognosis substantially. Despite the paradigm-shifting success of these novel treatments, their effectiveness is still limited by intrinsic or acquired resistance (3). Therefore, development of molecular imaging techniques able to precisely diagnose melanoma at the earliest practicable stage is crucial for improving the survival rate of patients with malignant disease (4).

Over recent decades, the imaging technologies of PET, SPECT, MRI, CT, and ultrasound have been studied in terms of their ability to detect melanoma. Of these, nuclear imaging technologies can visualize specific pathways or biomarkers of the melanoma disease process using molecular imaging probes. Several radiolabeled probes have been designed and evaluated for melanoma detection, including antibody-based imaging agents that show specific binding to melanoma, although technical limitations such as long residence time in the circulation and a slow penetration rate into the tumor were observed (5,6). N-isopropyl-p-^{123}I-iodoamphetamine was developed originally to measure cerebral blood flow and used to diagnose cerebrovascular diseases such as epilepsy and dementia. An unexpected benefit of N-isopropyl-p-^{123}I-iodoamphetamine is that after intravenous injection it is found in high concentrations in tissue regions producing melanin. However, detection of metastatic melanoma in the lungs and liver has proved difficult because N-isopropyl-p-^{123}I-iodoamphetamine shows high accumulation in these organs (7–10).

The benzamide structure has selective affinity for the pigment melanin, which is an irregular polymer produced by melanocytes (11). In malignant melanoma, the concentration of melanin increases substantially because elevated tyrosinase activity accelerates melanin biosynthesis. Many different radiolabeled benzamide derivatives have been investigated and reported for melanoma detection. During the initial stages of the research, [123]I- or ^{125}I-labeled benzamide derivatives were examined with respect to autoradiography or scintigraphy (12–15). These probes showed specific uptake by melanoma in vivo, revealing their potential as diagnostic probes. Following on from these, several ^{99m}Tc-complexes based on the

structural elements of benzamide were reported for melanoma detection using SPECT ([16–19]). These probes were evaluated in B16 murine melanoma–bearing mice and showed tumor-specific uptake; however, improvements to their targeting ability were needed before they could be applied in clinical trials. In recent years, the PET radionuclides ^{68}Ga and ^{18}F, which provide higher spatial resolution, have been used to radiolabel benzamide derivatives ([11,20–25]). Among them, ^{18}F-P3BZA was evaluated in melanoma patients as a preliminary clinical application and suggested a potential use for melanoma diagnosis ([26]). The skeleton structures of these probes are benzamide and aliphatic structures, including an alkyl linker and amine residue.

Here, we report the synthesis and characterization of N-(2-(dimethylamino)ethyl)-4-^{18}F-fluorobenzamide (^{18}F-DMFB) for early detection of metastatic melanoma using PET. We modified the structure of the benzamide derivatives to improve its ability to target melanoma. Biologic evaluations, including in vitro uptake, biodistribution, and small-animal PET studies, were performed on both metastatic melanoma and primary tumor models. Finally, we demonstrated the superiority of ^{18}F-DMFB as a novel PET agent for detecting metastatic malignant melanoma.

MATERIALS AND METHODS

Synthesis of ^{19}F-DMFB

The synthesis scheme for ^{19}F-DMFB is shown in Supplemental Figure 1 (supplemental materials are available at http://jnm.snmjournals. org). O-(N-succinimidyl)-1,1,3,3-tetramethyl-uronium tetrafluoroborate (215 mg, 0.714 mmol) and N,N-diisopropylethylamine (277 mg, 2.14 mmol) were added to a solution of 4-fluorobenzoic acid (100 mg, 0.714 mmol) in 5 mL of N,N-dimethylformamide. The reaction mixture was stirred for 3 h at 60°C and then cooled to room temperature. Subsequently, N,N-dimethylethylenediamine (107 mg, 1.21 mmol) was added to the reaction mixture. After stirring at room temperature for 2 h, the mixture was treated with H$_2$O and extracted with dichloromethane. After evaporation of the solvent, the crude mixture was purified using silica gel chromatography (dichloromethane:methanol = 10:1) and obtained as a yellow oil to yield 132 mg (88%) of ^{19}F-DMFB. ^{1}H nuclear MR (300 MHz, chloroform-d) δ (ppm) 2.23 (s, 6H), 4.48 (t, 2H, J = 3.6 Hz), 3.47 (q 2H), 7.0 (br, 1H), 7.04 (m, 3H), 7.79 (m, 2H). ^{13}C nuclear MR (75 MHz, chloroform-d) δ (ppm) 37.2, 45.1, 57.7, 115.4 (J = 12.75 Hz), 129.3 (J = 5.25 Hz), 130.7 (J = 2.25 Hz), 164.6 (J = 150 Hz), 166.4. High-resolution mass spectrometry (fast atom bombardment) m/z calculated for C$_{11}$H$_{15}$FN$_2$O [M+H]$^+$ = 211.1247; actual = 211.1246.

Radiolabeling of ^{18}F-DMFB

The chemical structures and synthesis scheme for ^{18}F-DMFB are shown in Figure 1 and Supplemental Figure 2. The N-succinimidyl-4-^{18}F-fluorobenzoate was prepared as described previously, with some modifications ([27]). Briefly, N,N-dimethylethylenediamine (7.6 mg, 86 μmol) was added to a solution of N-succinimidyl-4-^{18}F-fluorobenzoate in 0.2 mL of dimethyl sulfoxide. After stirring at 60°C for 30 min, the solution was cooled and injected into a semipreparative high-performance liquid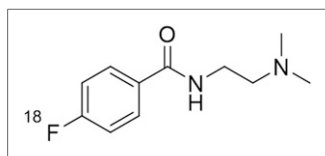 chromatography column system for purification. The mobile phase started with 100% solvent A (0.1% trifluoroacetic acid in water) and 0% solvent B (0.1% trifluoroacetic acid in acetonitrile) and ramped to 40% solvent A and 60% solvent B at 30 min; flow rate = 3 mL/min (retention time, 16.15 min).

FIGURE 1. Chemical structure of ^{18}F-DMFB.

Stability Study and In Vitro Binding Assay

The stability of ^{18}F-DMFB was analyzed by modification of a previously reported method ([28]). Instant thin-layer chromatography silica-gel strips were developed with dichloromethane and methanol (10:1) and were scanned. In vitro binding assays were performed as previously described ([23]).

Cell Culture and Cellular Uptake Studies

B16F10 (mouse melanoma), U87MG (human glioblastoma), and CT26 (mouse colon) cells were cultured in Dulbecco modified Eagle medium (B16F10, U87MG) or RPMI (CT26) supplemented with 10% fetal bovine serum. Cellular uptake studies were performed and calculated as previously described ([24]).

Preparation of Animal Models and Biodistribution Studies

Animal care, animal experiments, and euthanasia were performed in accordance with protocols approved by the Chonnam National University Animal Research Committee and the Guide for the Care and Use of Laboratory Animals ([29]). For the subcutaneous tumor models, Foxn1nu mice (5–6 wk old) were injected in the shoulder with B16F10 cells (1 × 10^6), CT26 cells (1 × 10^6), or U87MG cells (1 × 10^7). The lung metastases were created in C57BL/6 mice (5–6 wk old) via intravenous injection of B16F10 cells (2 × 10^5). The lymph node (LN) metastasis models were generated by injection of B16F10 cells (2 × 10^5 in 50 μL of Dulbecco phosphate-buffered saline) into the footpad of Foxn1nu mice for 2 min. The biodistribution studies in different organs were conducted 10, 30, 60, and 120 min after intravenous injection of 7.4 MBq of ^{18}F-DMFB into B16F10-bearing mice (n = 3/time point; tumor size, 100–150 mm^3).

Small-Animal PET

PET images were obtained using a high-resolution small-animal PET–SPECT/CT scanner (Inveon; Siemens Medical Solutions). PET studies of the tumor models (tumor size, 100–150 mm^3) were performed using an intravenous injection of ^{18}F-DMFB (7.4 MBq); images were acquired for 10 min. To compare ^{18}F-DMFB and ^{18}F-FDG images of melanoma, mouse models were injected with ^{18}F-DMFB 1 d after ^{18}F-FDG PET imaging. Regions of interest were drawn over the tumor, liver, and muscle on decay-corrected coronal images and analyzed. Acquired images were reconstructed with a 3-dimensional ordered-subset expectation-maximization algorithm, and image analysis was performed with PMOD software (PMOD Technologies Ltd.) ([30,31]). Uptake value was expressed as percentage injected dose (%ID)/g in coronal and transaxial PET images.

Statistical Analysis

The Mann–Whitney U test was used for statistical analysis. A P value of less than 0.05 was considered statistically significant. All data are expressed as mean ± SD.

RESULTS

Tracer Preparation and In Vitro Stability

^{19}F-DMFB was synthesized via 1-step procedures between 4-fluorobenzoic acid and N,N-dimethylethylenediamine. The cold form was separated by silica gel chromatography and analyzed by ^{1}H, ^{13}C nuclear MR, and high-resolution mass spectrometry to confirm its identity (Supplemental Fig. 2). The chemical yield of ^{19}F-DMFB was 75%. Different from cold synthesis, ^{18}F-DMFB was generated via coupling of the ^{18}F prosthetic group N-succinimidyl-4-^{18}F-fluorobenzoate to N,N-dimethylethylenediamine. The total labeling time of the ^{18}F-DMFB was within 140 min, including separation using high-performance liquid chromatography, and the overall decay-corrected radiochemical yield was approximately 15%–30%. The identity of ^{18}F-DMFB was confirmed by comparing the retention time with that of the reference compound (Supplemental Fig. 3). The specific activity of ^{18}F-DMFB was greater than 5.5 GBq/μmol.
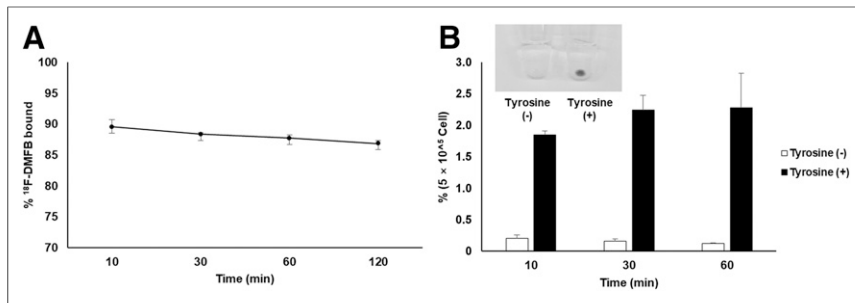
FIGURE 2. (A) In vitro binding of ^{18}F-DMFB to 2 mg of melanin at 37°C for 10, 30, 60, and 120 min. (B) In vitro uptake of ^{18}F-DMFB by B16F10 cells in presence and absence of L-tyrosine at 10, 30, and 60 min, including photograph of B16F10 cell pellets in absence (left) and presence (right) of L-tyrosine.

When the radiotracer was incubated in human serum at 37°C for 2 h, the percentage of the remaining ^{18}F-DMFB (R_f, 0.15–0.20) was greater than 95% (Supplemental Fig. 4).

In Vitro Binding and Cellular Uptake Studies

The binding affinity of ^{18}F-DMFB for melanin was assessed using commercial synthetic melanin (Fig. 2A). ^{18}F-DMFB showed high binding affinity for melanin (~90%) at 10 min after treatment, with binding retained for up to 2 h (86.84% ± 0.48%). Cell uptake studies of ^{18}F-DMFB were performed in the B16F10 cell line at 37°C for 1 h. Treatment with L-tyrosine (2 mM) stimulated the B16F10 cells and changed their color to black, with these black cells then being considered activated melanoma cells. Compared with inactivated B16F10 cells, the activated cells showed rapid and high accumulation of ^{18}F-DMFB at 10 min (1.84% ± 0.07% vs. 0.20% ± 0.06%), with uptake increasing for 1 h (2.28% ± 0.55% vs. 0.12% ± 0.01%) (Fig. 2B).

In Vivo Biodistribution Studies

The in vivo biodistribution of ^{18}F-DMFB was examined in B16F10 tumor–bearing Foxn1nu mice at 10, 30, 60, and 120 min after intravenous injection of ^{18}F-DMFB. A high level of radioactivity accumulated in the tumors, whereas activity in organs showed rapid washout. Tumor uptake of ^{18}F-DMFB was greater than 9 % ID/g at 10 min after radiotracer injection and 13 %ID/g at 1 h (Table 1). The tumor-to-skin, -lung, -brain, -liver, -bone, and -intestine ratios were 6.54 ± 1.02, 7.13 ± 2.44, 12.20 ± 5.00, 5.54 ± 1.27, 13.73 ± 5.87, and 4.90 ± 0.22, respectively, at 1 h after ^{18}F-DMFB injection (Supplemental Table. 1). Notably, these ratios increased to at least 20-fold at 2 h after radiotracer injection.

PET Imaging Studies of ^{18}F-DMFB

Static PET studies of ^{18}F-DMFB were performed on B16F10-bearing Foxn1nu mice, as well as on CT26 or U87MG xenografts. B16F10 tumors could be visualized clearly at 10 min after injection, and tumor uptake increased for 1 h, with excellent tumor-to-background contrast (7.39 ± 0.89 %ID/g at 1 h, Fig. 3A). There was no uptake in lung or liver after 30 min. In addition, only B16F10 tumors were specifically visualized when PET studies were performed with B16F10 (8.49 %ID/g) and CT26 (0.85 %ID/g), or B16F10 (8.34 %ID/g) and U87MG (0.83 %ID/g), cell–bearing Foxn1nu mice (Figs. 3B and 3C).

In PET imaging studies of the lung metastasis models, good visualization of the metastatic region was obtained 1 h after intravenous injection of ^{18}F-DMFB. Representative maximum-intensity-projection and axial images of normal and metastatic mouse models collected between 60 and 70 min after ^{18}F-DMFB injection are shown in Figures 4A and 4B. Region-of-interest analysis showed that normal lung uptake of ^{18}F-DMFB was 0.53 ± 0.13 %ID/g, whereas uptake in lung metastasis was 6.58 ± 1.63 %ID/g (n = 11, $P < 0.001$, Supplemental Fig. 5). Furthermore, a 1.93-mm–sized

TABLE 1
Biodistribution of ^{18}F-DMFB in Foxn1nu Mice Bearing B16F10 After Intravenous Injection

Site	10 min	30 min	60 min	120 min
Blood	5.26 ± 1.02	3.20 ± 0.51	0.98 ± 0.26	0.16 ± 0.006
Heart	6.22 ± 0.91	3.07 ± 0.17	1.20 ± 0.38	0.20 ± 0.024
Lung	11.66 ± 2.91	4.57 ± 0.65	1.89 ± 0.63	0.33 ± 0.031
Liver	11.19 ± 0.62	5.76 ± 0.41	2.47 ± 1.05	0.45 ± 0.06
Spleen	13.19 ± 2.58	5.88 ± 0.83	2.23 ± 0.92	0.34 ± 0.12
Stomach	9.01 ± 4.51	6.49 ± 2.35	2.87 ± 0.29	0.82 ± 0.64
Intestine	12.54 ± 1.56	7.88 ± 0.82	2.65 ± 0.80	0.52 ± 0.09
Kidney	40.42 ± 14.69	16.74 ± 4.91	5.08 ± 1.69	0.93 ± 0.29
Pancreas	10.03 ± 3.20	4.73 ± 0.62	1.77 ± 0.78	0.20 ± 0.05
Muscle	5.67 ± 0.60	3.36 ± 1.68	1.44 ± 0.11	0.34 ± 0.12
Bone	5.07 ± 0.38	2.40 ± 0.40	1.03 ± 0.47	0
Brain	6.84 ± 1.02	2.96 ± 0.61	1.21 ± 0.70	0.26 ± 0.08
Skin	7.73 ± 1.63	3.94 ± 1.73	1.96 ± 0.32	0.37 ± 0.07
Eyes	4.26 ± 0.50	2.79 ± 0.71	1.05 ± 0.07	0.04 ± 0.02
Tumor	9.24 ± 2.23	10.80 ± 3.27	13.00 ± 3.90	10.59 ± 1.35

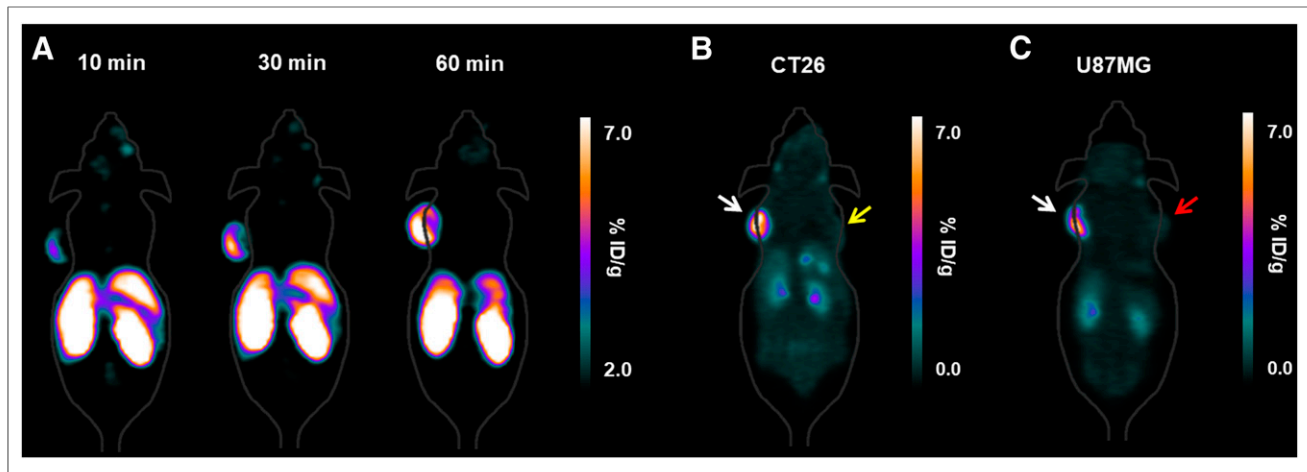Data are %ID/g ± SD (n = 3/time point).

FIGURE 3. (A) PET images of mice bearing B16F10 at 10, 30, and 60 min after injection of ^{18}F-DMFB. (B and C) PET images of mice bearing B16F10 and CT26 (B) and B16F10 and U87MG (C) at 60 min after injection of ^{18}F-DMFB (white arrow, B16F10; yellow arrow, CT26; red arrow, U87MG).

liver metastasis of melanoma was incidentally visualized by ^{18}F-DMFB PET (Fig. 4C).

On the basis of the PET imaging results from lung metastasis models, we further investigated the ability of ^{18}F-DMFB to visualize LNs harboring metastatic malignant melanoma in mouse models. LN metastasis models were established in Foxn1nu mice by direct injection of B16F10 cells into the foot pad. Twenty-one days after cancer cell injection, over 70% of the mice had black LNs in the popliteal area (Fig. 5A). As shown in Figure 5B, small metastatic popliteal LNs (<4 mm) were clearly visualized by ^{18}F-DMFB PET, with a high signal-to-background ratio. Finally, metastatic LNs were confirmed by histopathologic analysis (Fig. 5C). Furthermore, we evaluated the sensitivity of ^{18}F-DMFB to metastatic popliteal LNs of different sizes. All LN metastases (size range, 1–7.5 mm; $n = 5$) were homogeneously visualized by ^{18}F-DMFB, regardless of tumor size (Supplemental Fig. 6).

Finally, we compared PET images of ^{18}F-DMFB and ^{18}F-FDG in B16F10-bearing Foxn1nu mice and lung metastasis models. B16F10 tumors were visualized clearly by each radiotracer at 60 min after intravenous injection; however, different patterns of biodistribution were observed (Fig. 6A). ^{18}F-DMFB accumulated

in tumors and was otherwise rapidly washed out through the bladder, whereas ^{18}F-FDG showed uptake in brain, heart, liver, tumor, and bladder. The tumor-to-liver uptake ratios of ^{18}F-DMFB and ^{18}F-FDG at 60 min were 8.04 ± 0.81 and 5.04 ± 1.43, respectively ($n = 9$, $P < 0.01$), whereas the tumor-to-muscle uptake ratios were 15.21 ± 1.58 and 13.03 ± 2.40, respectively ($n = 9$, $P < 0.05$). Similar patterns were shown for PET imaging of each tracer in the lung metastasis models. Lung metastases imaged by ^{18}F-DMFB showed excellent metastasis-to-background contrast, whereas metastases were not prominent on ^{18}F-FDG imaging because of high background activity in brown adipose tissue and heart (Fig. 6B).

DISCUSSION

Metastasis is a representative characteristic of malignant melanoma and is the cause of most melanoma-related deaths. The survival rate of malignant melanoma depends on the extent of the disease; if the malignant melanoma is localized, 5-y survival is 90%; however, if the tumor has metastasized at the time of diagnosis, 5-y survival is only 6%. Thus, accurate diagnosis of the tumor location at an early stage is crucial for increasing
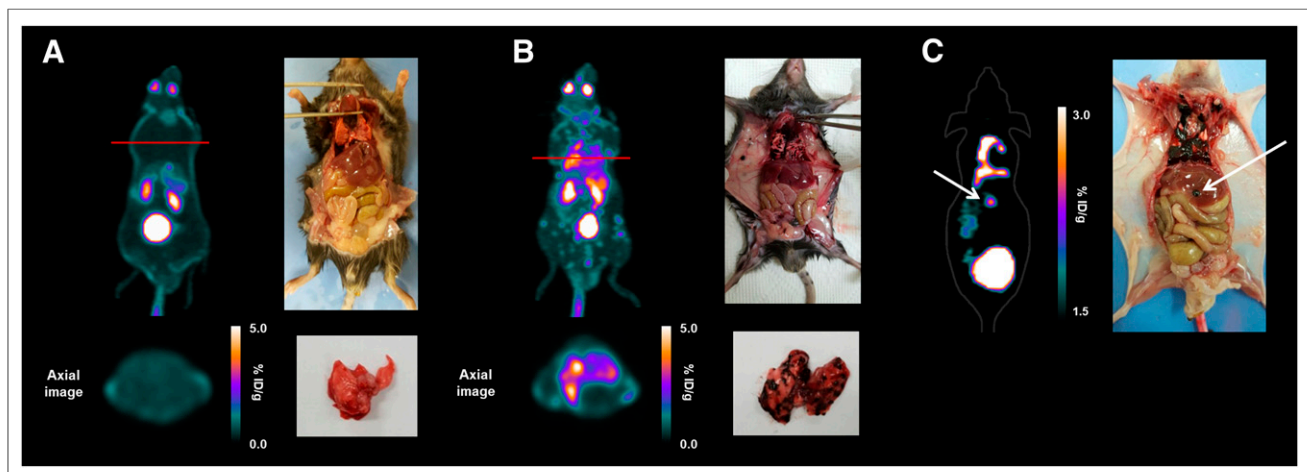

FIGURE 4. (A and B) Maximum-intensity-projection (top) and transaxial (bottom) images of normal (A) and lung metastasis (B) model (C57BL/6) at 60 min after injection of ^{18}F-DMFB. (C) Coronal PET image of B16F10 liver metastasis model (Foxn1nu) at 60 min after injection of ^{18}F-DMFB.
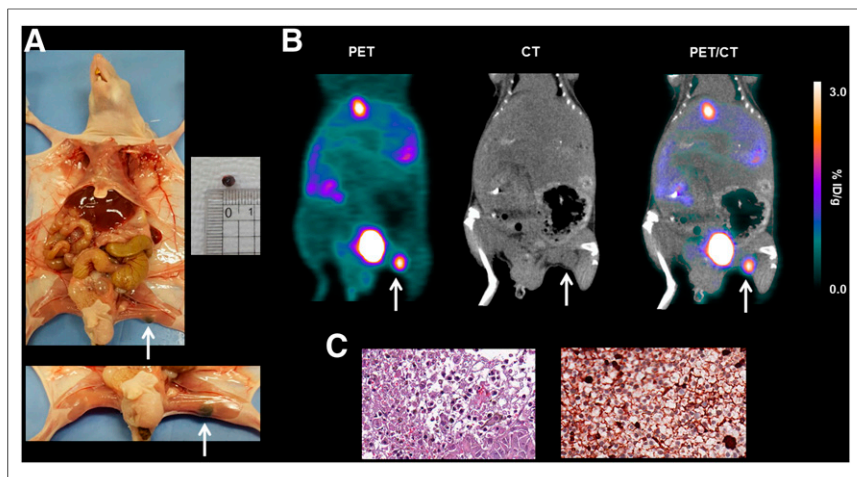
FIGURE 5. (A) Photograph of B16F10 LN metastasis model. (B) PET, CT, and PET/CT images of B16F10 LN metastasis model at 60 min after injection of ^{18}F-DMFB. (C) Photomicrographs of LN metastasis. (White arrows, LN metastasis region.)

the probability of survival. In this study, we synthesized a novel ^{18}F-labeled benzamide derivative to target melanin with high affinity and evaluated its in vitro and in vivo performance.

Benzamide derivatives for PET comprise radiolabeled benzamide and an aliphatic structure that includes an alkyl linker and an amine residue (11,21–25,32,33). Many researchers have modified the structure, especially the benzene ring, to improve radiochemical yield, melanin-targeting ability, or pharmacokinetic properties. Although radiochemical yield was improved, biodistribution studies in mice show that the melanoma uptake of these PET probes is less than 10 %ID/g at 60 min. Instead, we focused on the amine residue of the benzamide derivatives because melanin can be targeted by aliphatic structures such as the N,N-diethylethylenediamine group (34). Finally, we changed the amine residue from ethyl to methyl, which resulted in high sensitivity for melanoma detection.

Our cellular and in vivo results indicate that ^{18}F-DMFB has good potential as a molecular probe to detect melanoma, with high stability and specificity. The in vivo biodistribution study revealed rapid and high accumulation of ^{18}F-DMFB in the tumor, with stable

retention for at least 2 h. Previously, N-[2-(diethylamino)-ethyl]-4-^{18}F-fluorobenzamide, which has a benzamide structure with a diethyl amine residue, showed approximately 6 %ID/g tumor uptake at 1 h after injection (11,25). However, ^{18}F-DMFB showed 2-fold higher tumor uptake than the previous compound at 1 h (13.00 ± 3.90 %ID/g). Rapid washout from all examined organs, but not from the tumor, resulted in high tumor-to-organ ratios. Tumor-to-skin, -lung, -liver, -bone, and -intestine ratios are particularly important when developing a PET agent for malignant melanoma because these organs are common sites for metastasis (35). Interestingly, brain uptake of ^{18}F-DMFB was observed at 1 and 2 h after injection (1.21 ± 0.70 and 0.26 ± 0.08 %ID/g, respectively), which means that ^{18}F-DMFB can penetrate the blood–brain barrier. Previous publications reported that in B16F10-bearing mice, the tumor-to-brain ratio of ^{18}F-FDG was 2.86 ± 0.35 at 1 h (11). However, the tumor-to-brain ratio of ^{18}F-DMFB reached over 12 because of the low normal-brain uptake of ^{18}F-DMFB; this result demonstrates the potential of ^{18}F-DMFB for imaging of melanoma brain metastases.

In this respect, ^{18}F-DMFB has excellent in vivo properties as a PET probe to diagnose malignant melanoma. The biodistribution results were confirmed by PET imaging, with tumors becoming visible about 10 min after ^{18}F-DMFB injection and uptake continuing to increase up until 1 h. Melanin specificity was also confirmed by PET imaging in non–melanoma-bearing Foxn1nu mice.

A main goal of the present study was to investigate the feasibility of ^{18}F-DMFB for detecting melanoma metastasis. This was evaluated using murine models of lung, liver, and LN metastasis. We found that uptake of ^{18}F-DMFB was more than 12-fold higher in metastatic lung than in normal lung. The tumor-to-lung or tumor-to-liver ratios of ^{18}F-DMFB were high in the biodistribution study, and a small liver metastasis was clearly visualized at 1 h on PET imaging, with fast washout from the liver. Comparison studies of ^{18}F-DMFB and ^{18}F-FDG revealed that the tumor uptake of ^{18}F-DMFB was lower than that of ^{18}F-FDG. However, the biodistribution of ^{18}F-DMFB was better than that of ^{18}F-FDG, which resulted in excellent tumor-to-background contrast. In particular, detection of lung metastases is difficult on ^{18}F-FDG PET because they can be masked by high uptake in the heart.

In addition, ^{18}F-DMFB demonstrated clear detection of LN metastasis. Regional LN status is the most important prognostic factor for malignant melanoma patients because the lymphatic system is invariably involved in spreading melanoma (36,37). Tumor cells enter a lymphatic vessel, transit through a LN, and then enter the systemic circulation via the thoracic duct (35).

In the present study, we demonstrated the excellent image quality of ^{18}F-DMFB
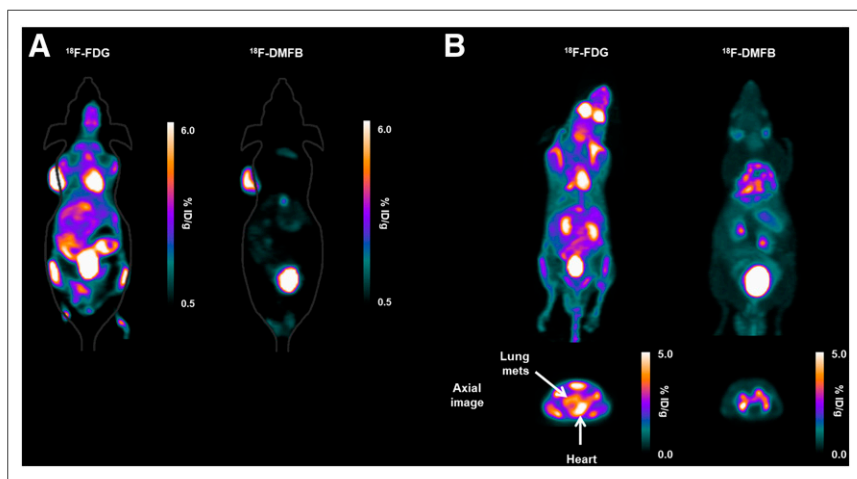

FIGURE 6. PET imaging of ^{18}F-FDG and ^{18}F-DMFB in mouse models. (A) Coronal images in mice bearing B16F10 at 60 min after injection. (B) Maximum-intensity-projection (top) and transaxial (bottom) images of lung metastasis model at 60 min after injection. mets = metastases.

for detecting primary and metastatic melanoma. However, it is reported that picolinamide derivatives show higher performance for malignant melanoma than benzamide derivatives (*4*). Therefore, we think that picolinamide derivatives with a dimethyl amine residue may show better performance with respect to diagnosis of metastatic malignant melanoma.

CONCLUSION

^{18}F-DMFB was easily synthesized via a coupling reaction, and its in vitro and in vivo characteristics were evaluated. The rapid and prolonged retention of ^{18}F-DMFB in melanoma, but not in normal organs, suggests that this labeled probe can be used as an imaging agent to obtain high-contrast PET images of melanoma shortly after its injection. The excellent in vivo kinetics and specific tumor uptake warrant its further investigation for imaging of melanoma, with ^{18}F-DMFB having the potential to be a novel molecular probe for the PET-based diagnosis of malignant melanoma and its metastasis.

DISCLOSURE

ACKNOWLEDGMENTS

REFERENCES

1. Garbe C, Peris K, Hauschild A, et al. Diagnosis and treatment of melanoma: European consensus-based interdisciplinary guideline—update 2016. *Eur J Cancer.* 2016;63:201–217.
2. Harries M, Malvehy J, Lebbe C, et al. Treatment patterns of advanced malignant melanoma (stage III-IV): a review of current standards in Europe. *Eur J Cancer.* 2016;60:179–189.
3. Henriques V, Martins T, Link W, Ferreira BI. The emerging therapeutic landscape of advanced melanoma. *Curr Pharm Des.* 2018;24:549–558.
4. Liu H, Liu S, Miao Z, et al. Development of ^{18}F-labeled picolinamide probes for PET imaging of malignant melanoma. *J Med Chem.* 2013;56:895–901.
5. Vavere AL, Butch ER, Dearling JL, et al. [64]Cu-*p*-NH2-Bn-DOTA-hu14.18K322A, a PET radiotracer targeting neuroblastoma and melanoma. *J Nucl Med.* 2012;53:1772–1778.
6. Voss SD, Smith SV, DiBartolo N, et al. Positron emission tomography (PET) imaging of neuroblastoma and melanoma with ^{64}Cu-SarAr immunoconjugates. *Proc Natl Acad Sci USA.* 2007;104:17489–17493.
7. Ito Y, Doi H, Tsuji H, Ishida-Yamamto A, Iizuka H. Malignant melanoma of the breast: *N*-isopropyl-*p*-^{123}I-iodoamphetamine single photon emission computed tomography (^{123}I-IMP SPECT) is useful for the detection of metastasis. *J Dermatol.* 2010;37:849–851.
8. Yoshimura M, Kanesaka N, Saito K, Koizumi K, Tokuuye K, Goto H. Diagnosis of uveal malignant melanoma by a new semiquantitative assessment of *N*-isopropyl-*p*-^{123}I-iodoamphetamine. *Jpn J Ophthalmol.* 2011;55:148–154.
9. Sou R, Oku N, Ohguro N, Hibino S, Fujikado T, Tano Y. The clinical role of *N*-isopropyl-*p*-^{123}I-iodoamphetamine single photon emission computed tomography in the follow-up of choroidal melanoma after radiotherapy. *Jpn J Ophthalmol.* 2004;48:54–58.
10. Holman BL, Wick MM, Kaplan ML, et al. The relationship of the eye uptake of *N*-isopropyl-*p*-[^{123}I]iodoamphetamine to melanin production. *J Nucl Med.* 1984;25:315–319.
11. Ren G, Miao Z, Liu H, et al. Melanin-targeted preclinical PET imaging of melanoma metastasis. *J Nucl Med.* 2009;50:1692–1699.
12. Michelot JM, Moreau MF, Labarre PG, et al. Synthesis and evaluation of new iodine-125 radiopharmaceuticals as potential tracers for malignant melanoma. *J Nucl Med.* 1991;32:1573–1580.
13. Maffioli L, Mascheroni L, Mongioj V, et al. Scintigraphic detection of melanoma metastases with a radiolabeled benzamide ([iodine-123]-(S)-IBZM). *J Nucl Med.* 1994;35:1741–1747.
14. Michelot JM, Moreau MF, Veyre AJ, et al. Phase II scintigraphic clinical trial of malignant melanoma and metastases with iodine-123-*N*-(2-diethylaminoethyl 4-iodobenzamide). *J Nucl Med.* 1993;34:1260–1266.
15. Nicholl C, Mohammed A, Hull WE, Bubeck B, Eisenhut M. Pharmacokinetics of iodine-123-IMBA for melanoma imaging. *J Nucl Med.* 1997;38:127–133.
16. Auzeloux P, Moreau MF, Papon J, et al. Technetium-99m radiolabelling of an *N*-amino-alkyl-benzamide nitrido- and oxo-technetium bis(aminoethanethiol) derivative synthesis and biological results: potential melanoma tracer agents. *J Labelled Comp Radiopharm.* 1999;42:567–579.
17. Auzeloux P, Papon J, Masnada T, et al. Synthesis and biodistribution of technetium-99m-labelled *N*-(diethylaminoethyl)benzamide via a bis(dithiocarbamate) nitridotechnetium(V) complex. *J Labelled Comp Radiopharm.* 1999;42:325–335.
18. Auzeloux P, Papon J, Azim EM, et al. A potential melanoma tracer: synthesis, radiolabeling, and biodistribution in mice of a new nitridotechnetium bis(aminothiol) derivative pharmacomodulated by a *N*-(diethylaminoethyl)benzamide. *J Med Chem.* 2000;43:190–198.
19. Auzeloux P, Papon J, Pasqualini R, Madelmont JC. Synthesis and biodistribution of a new oxo-technetium-99m bis(aminothiol) complex as a potential melanoma tracer. *J Med Chem.* 2001;44:1116–1121.
20. Kertész I, Vida A, Nagy G, et al. In vivo imaging of experimental melanoma tumors using the novel radiotracer ^{68}Ga-NODAGA-procainamide (PCA). *J Cancer.* 2017;8:774–785.
21. Trencsényi G, Denes N, Nagy G, et al. Comparative preclinical evaluation of ^{68}Ga-NODAGA and ^{68}Ga-HBED-CC conjugated procainamide in melanoma imaging. *J Pharm Biomed Anal.* 2017;139:54–64.
22. Chang CC, Chang CH, Lo YH, et al. Preparation and characterization of a novel Al[18]F-NOTA-BZA conjugate for melanin-targeted imaging of malignant melanoma. *Bioorg Med Chem Lett.* 2016;26:4133–4139.
23. Kim HJ, Kim DY, Park JH, et al. Synthesis and characterization of a ^{68}Ga-labeled *N*-(2-diethylaminoethyl)benzamide derivative as potential PET probe for malignant melanoma. *Bioorg Med Chem.* 2012;20:4915–4920.
24. Kim HJ, Kim DY, Park JH, et al. Synthesis and evaluation of a novel ^{68}Ga-labeled DOTA-benzamide derivative for malignant melanoma imaging. *Bioorg Med Chem Lett.* 2012;22:5288–5292.
25. Garg S, Kothari K, Thopate SR, Doke AK, Garg PK. Design, synthesis, and preliminary in vitro and in vivo evaluation of *N*-(2-diethylaminoethyl)-4-[^{18}F] fluorobenzamide ([^{18}F]-DAFBA): a novel potential PET probe to image melanoma tumors. *Bioconjug Chem.* 2009;20:583–590.
26. Ma X, Wang S, Wang S, et al. Biodistribution, radiation dosimetry, and clinical application of a melanin-targeted PET probe, ^{18}F-P3BZA, in patients. *J Nucl Med.* 2019;60:16–22.
27. Tang G, Tang X, Wangb X. A facile automated synthesis of *N*-succinimidyl 4-[^{18}F]fluorobenzoate ([^{18}F]SFB) for ^{18}F-labeled cell-penetrating peptide as PET tracer. *J Labelled Comp Radiopharm.* 2010;53:543–547.
28. Yun M, Kim DY, Lee JJ, et al. A high-affinity repebody for molecular imaging of EGFR-expressing malignant tumors. *Theranostics.* 2017;7:2620–2633.
29. *Guide for the Care and Use of Laboratory Animals.* 8th ed. Washington, DC: National Academy Press; 2011.
30. Blasi F, Oliveira BL, Rietz TA, et al. Effect of chelate type and radioisotope on the imaging efficacy of 4 fibrin-specific PET probes. *J Nucl Med.* 2014;55:1157–1163.
31. Sah BR, Schibli R, Waibel R, et al. Tumor imaging in patients with advanced tumors using a new ^{99m}Tc-radiolabeled vitamin B12 derivative. *J Nucl Med.* 2014;55:43–49.
32. Denoyer D, Greguric I, Roselt P, et al. High-contrast PET of melanoma using ^{18}F-MEL050, a selective probe for melanin with predominantly renal clearance. *J Nucl Med.* 2010;51:441–447.
33. Wu SY, Huang SP, Lo YC, et al. Synthesis and preclinical characterization of [^{18}F] FPBZA: a novel PET probe for melanoma. *BioMed Res Int.* 2014;2014:912498.
34. Liu H, Liu SL, Miao Z, et al. A novel aliphatic ^{18}F-labeled probe for PET imaging of melanoma. *Mol Pharm.* 2013;10:3384–3391.
35. Damsky WE, Rosenbaum LE, Bosenberg M. Decoding melanoma metastasis. *Cancers (Basel).* 2010;3:126–163.
36. Pasquali S, Mocellin S, Campana LG, et al. Early (sentinel lymph node biopsy-guided) versus delayed lymphadenectomy in melanoma patients with lymph node metastases: personal experience and literature meta-analysis. *Cancer.* 2010;116:1201–1209.
37. Thomas JM. Sentinel lymph node biopsy in malignant melanoma. *BMJ.* 2008;336:902–903.